

On-Surface Activation of Trimethylsilyl-Terminated Alkynes on Coinage Metal Surfaces

Liding Zhang,^[a] Yi-Qi Zhang,^[a] Zhi Chen,^[b] Tao Lin,^[a, c] Mateusz Paszkiewicz,^[a] Raphael Hellwig,^[a] Tianjiao Huang,^[a] Mario Ruben,^[b, d] Johannes V. Barth,^[a] and Florian Klappenberger*^[a]

The controlled attachment of protecting groups combined with the ability to selectively abstract them is central to organic synthesis. The trimethylsilyl (TMS) functional group is a popular protecting group in solution. However, insights on its activation behavior under ultra-high vacuum (UHV) and surface-confined conditions are scarce. Here we investigate a series of TMS-protected alkyne precursors via scanning tunneling microscopy (STM) regarding their compatibility with organic molecular beam epitaxy (OMBE) and their potential deprotection on various coinage metal surfaces. After in-situ evaporation on the substrates held in UHV at room temperature, we find that all molecules arrived and adsorbed as intact units forming ordered supramolecular aggregates stabilized by non-covalent interac-

tions. Thus, TMS-functionalized alkyne precursors with weights up to 1100 atomic mass units are stable against OMBE evaporation in UHV. Furthermore, the TMS activation through thermal annealing is investigated with STM and X-ray photoelectron spectroscopy (XPS). We observe that deprotection starts to occur between 400 K and 500 K on the copper and gold surfaces, respectively. In contrast, on silver surfaces, the TMS-alkyne bond remains stable up to temperatures where molecular desorption sets in (≈ 600 K). Hence, TMS functional groups can be utilized as leaving groups on copper and gold surfaces while they serve as protecting groups on silver surfaces.

1. Introduction

The success of carbon-nanotubes and graphene^[1] in recent years has made the synthesis of novel one-dimensional (1D) and two-dimensional (2D) carbon-nanomaterials the subject of intense efforts in scientific research.^[2,3] The main drive behind this movement originates from the outstanding mechanical and electronic properties of graphene and other 2D materials promising a plethora of new applications in a wide range of fields. Recently, in addition to the popular sp^2 carbon materials, also 1D and 2D carbon-allotropes such as graphyne and graphdiyne have gained widespread attention because of their potential to outrival graphene regarding specific applications partly due to their inherent semiconducting electronic properties and nanoporous structures.^[4–8] Yet, the reliable fabrication of such structures with desired purity still remains challenging.

The surface-assisted bottom-up fabrication of nanomaterials utilizing rationally designed molecular precursors as building blocks which are assembled on metal surfaces represents an attractive alternative to traditional wet-chemistry because it offers access to high quality products achieved through new reaction pathways.^[9–18] Precursors carrying alkyne functional groups express an intriguingly rich surface chemistry^[19] including dehydrogenation,^[20] homo-coupling,^[21,22] cross-coupling,^[23–25] cyclotrimerization,^[26,27] and metathesis reactions^[28] as well as the formation of enyne,^[27,29] metal-organic,^[30,31] and organometallic linkages.^[32–35] They constitute promising building-blocks for the surface-guided construction of low-dimensional architectures^[36] partly expressing covalent character.^[16,37–39] Unfolding their full potential is, however, frequently limited by unwanted side-reactions^[16,40,41] resulting from the rich chemical conversion possibilities, thus raising demands for increased control through template-driven protocols and optimized precursor design.

In organic synthesis, the utilization of different chemical moieties as leaving and protecting groups for developing precise molecular precursors is an essential and widely used tool^[42] for steering reaction pathways. While halogens usually act as leaving groups in Ullmann or Sonogashira coupling reactions, organosilicon groups such as trimethylsilyl (TMS) are commonly employed as protecting groups.^[43,44] In on-surface synthesis, aryl halides are a wide-spread choice^[10,15,36,45,46] for controlling coupling processes. By contrast, investigations dealing with precursors comprising TMS groups under interfacial conditions are scarce,^[28,47,48] and therefore knowledge on their activation conditions is missing.

[a] L. Zhang, Dr. Y.-Q. Zhang, Dr. T. Lin, M. Paszkiewicz, Dr. R. Hellwig, T. Huang, Prof. Dr. J. V. Barth, Dr. F. Klappenberger
Physics Department E20, Technical University of Munich (TUM), 85748 Garching, Germany
E-mail: florian.klappenberge@tum.de

[b] Dr. Z. Chen, Prof. Dr. M. Ruben
Institute of Nanotechnology (INT), Karlsruhe Institute of Technology (KIT), 76344 Eggenstein-Leopoldshafen, Germany

[c] Dr. T. Lin
College of New Materials and New Energies, Shenzhen Technology University, 518118 Shenzhen, China

[d] Prof. Dr. M. Ruben
Département des Matériaux Organiques (DMO), Institut de Physique et Chimie des Matériaux de Strasbourg (IPCMS), 67034 Strasbourg, France

Supporting information for this article is available on the WWW under <https://doi.org/10.1002/cphc.201900249>

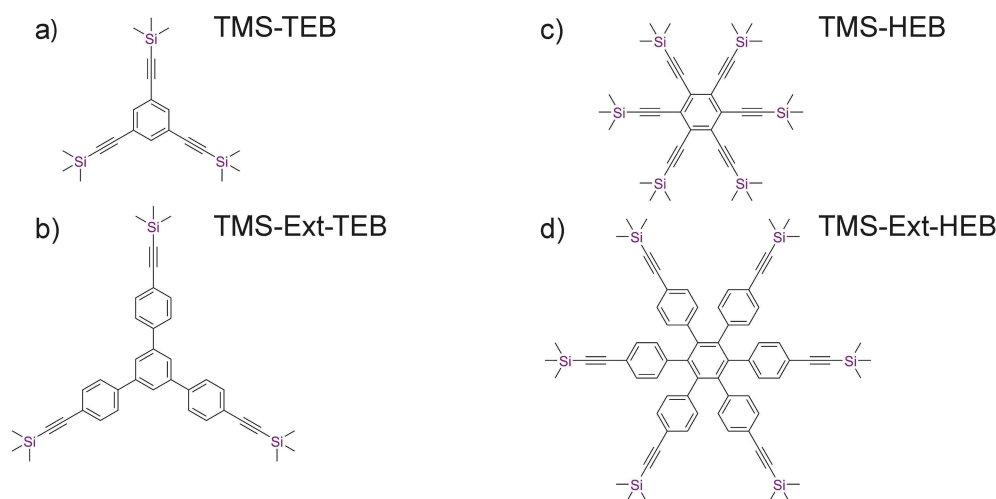


Figure 1. Overview of the employed TMS building blocks.

Organic molecular beam epitaxy (OMBE) is the method of choice for the in-situ evaporation of organic material under ultra-high vacuum (UHV) conditions because it affords the highest purity of deposited material. However, it requires that the employed molecules can be heated to their sublimation temperature without deteriorating. Thus, despite sophisticated and complex alkyne precursors being in principle available through solution synthesis, their utilization is limited by the reactivity of the ethynyl groups leading to polymerization in the Knudsen cell and thus preventing evaporation. Therefore, during our previous work, we were limited to studying smaller alkyne derivatives with atomic weights typically below 300 g/mol. Drop casting is an alternative deposition technique that circumvents this particular restriction, but has its own limitations. Samples prepared with this method suffer from inhomogeneities in the spatial distribution of the deposited material by cluster formation inside the solvent and contamination due to residuals from the synthesis and solvent-substrate-atmosphere interactions during the casting process.^[49,50]

Here we investigate with scanning tunneling microscopy (STM) and X-ray photoelectron spectroscopy (XPS) the properties of TMS-functionalized alkyne derivatives regarding their compatibility with the OMBE evaporation process and the character of the TMS-functional group, ranging from protecting to leaving group, depending on the supporting metal surfaces. For this reason, we studied the evaporation and activation behavior of the following TMS-functionalized molecules on the Cu(111), Ag(111), Ag(877) and Au(111) and surfaces:

- 1,3,5-Tris-[trimethylsilylethynyl]-benzene (TMS-TEB)
- 1,3,5-Tris-[4-(trimethylsilylethynyl)phenyl]-benzene (TMS-Ext-TEB)
- 1,2,3,4,5,6-Hexakis-[trimethylsilylethynyl]-benzene (TMS-HEB)
- 1,2,3,4,5,6-Hexakis-[4-(trimethylsilylethynyl)phenyl]-benzene (TMS-Ext-HEB)

The structures of these molecules are depicted in Figure 1. We demonstrate that all species adsorb on the crystal surfaces as intact units, and thus can be successfully evaporated using

OMBE, and that after adsorption, most molecules self-assemble into densely-packed, highly regular domains, whereby their structures can be rationalized through non-covalent intermolecular interactions. Furthermore, by a series of thermal treatment protocols systematically increasing the annealing temperature, we reveal that regarding potential deprotection, the TMS moieties behave similar to typical protecting and leaving groups depending on the nature of the substrate. Specifically, on Cu and Au the functional groups can be cleaved off by gentle annealing, while on Ag comparably high temperatures leave the organosilicon units unchanged.

Experimental Section

STM Measurements. The STM measurements were carried out in two different setups: a home-built Besocke-type STM and a commercial Joule-Thomson STM (JT-STM, SPECS), with base pressure better than 1×10^{-10} in both setups. The Cu(111), Ag(111), Au(111), and Ag(877) crystals were prepared by repeated sputtering with ionized argon gas and subsequent annealing cycles in order to achieve clean surfaces with smooth and extended terraces. All molecules were evaporated onto the crystals by means of OMBE from a quartz crucible at the respective temperatures listed in Table 1.

XPS Measurements. The XPS data was recorded at the HE-SGM beamline of the BESSY-II synchrotron facility in Berlin, Germany. All measurements were performed at a base pressure in the 10^{-10} mbar regime. Samples were prepared using the same methods as for samples investigated via STM. For the XPS spectra, excitation energies of 435 eV and 200 eV were used for the C 1s

Table 1. Overview of the respective sublimation temperatures.

Molecule	Weight [g/mol]	Sublimation temperature [K]
TMS-Ext-HEB	1111.93	533
TMS-HEB	655.34	420
TMS-Ext-TEB	595.02	445
TMS-TEB	366.73	293

and Si 2p regions, respectively. The analyzer was operated with a pass energy of 20 eV. All measured spectra were acquired under normal emission of the detected electrons. For the calibration of the binding energies, the Cu 3p_{3/2} line of the substrate at 75.04 eV and Ag 3d_{5/2} line at 368.30 eV was used, respectively.

Synthesis Protocols. For information on molecule synthesis kindly refer to the supporting information.

Molecular Models. Superpositioned molecule structures were simulated with HyperChem 7.0 using the semi-empirical AM1 method.

2. Results and Discussion

2.1. TMS-TEB

The starting point of our experiments was TMS-TEB (cf. Figure 1a), a comparably small species (367 g/mol), with a central phenyl ring and three TMS-protected alkyne moieties attached in three-fold symmetric positions.

2.1.1. Cu(111)

After deposition of TMS-TEB onto a Cu(111) crystal held at 200 K, scattered isolated molecules are present on the surface together with a minority of small aggregates (Figure 2a). Superpositioning molecular models onto a cluster (Figure 2a inset) indicates that intact organic units appear as triangle-shaped objects with a bright feature at each corner. We attribute the bright features to the TMS groups. The uniform appearance of the individual organic units demonstrates that the molecules have reached the surface intact and thus that TMS groups have not been cleaved off, neither during evaporation nor adsorption. The absence of ordered domains indicates a significant interaction with the substrate, strong enough to suppress surface diffusion to a large extent. Interestingly, with a few exceptions, all TMS-TEB units exhibit the same orientation with respect to the high symmetry directions. This hints towards an adsorption configuration of the three-fold symmetric adsorbate being sensitive to the second layer of the substrate.^[51] Since TMS-TEB is a three-fold symmetric molecule, if only the interaction between a molecule and the six-fold symmetric top-most layer (A-layer) of the Cu(111) surface were decisive, two equal adsorption configurations rotated by 60° against each other would be expected. However, the fcc-type stacking of the top-most layer (A-layer) with the second layer (B-layer) of the Cu(111) surface (Figure 2c) reduces the symmetry of the substrate to a three-fold symmetry. Then, two distinctly different adsorption configurations 1 and 2 can be distinguished, of which one is favored (Figure 2d).

After annealing the sample to 400 K (Figure 2b), irregular aggregates presenting features with reduced apparent height have formed in which identifying individual molecules is challenging. A few remaining isolated molecules are observable. As the bright features originate from the size of the TMS

groups, the appearance of novel species with reduced apparent height is attributed to the abstraction of TMS groups due to thermal cleavage of the alkynyl-Si bond during the annealing process.

Subsequently, the same sample was annealed to 500 K. As a result, isolated monomer units have disappeared and connected structures of uniform height with embedded bright features have formed (Figure S5a). In contrast to the previous step, the relative amount of the prominent protrusions has clearly decreased. While our data suggests that TMS-protection groups have been abstracted from their TEB backbone, neither isolated units nor densely packed islands of these bright features can be observed.

To obtain a clearer chemical picture of the abstraction, we carried out XPS measurements. We prepared a sample featuring a submonolayer coverage (~0.5 ML) of TMS-TEB on Cu(111) and investigated the C 1s and the Si 2p regions for annealing temperatures up to 500 K. For the 300 K case, the Si 2p spectra (Figure 3a, blue) are dominated by the spin-orbit split double feature of a single TMS group at a binding energy of 100.5 eV for the 2p_{3/2} peak that is in agreement with carbon-bound TMS groups.^[52,53] After 450 K annealing (green), the peak intensity is reduced by more than two thirds indicating that Si-containing groups desorb from the surface. After 500 K annealing, approximately 25% of the signal remain, featuring a binding energy of 99.2 eV typical for atomic and neutral Si atoms.^[52,54] Furthermore, we quantified the ratio by which the integrated counts decreased for the C 1s region (Figure S6). After annealing to 500 K the total carbon count has decreased to around 61%. Assuming a full deprotection of the alkynyl groups, a reduction of the C 1s intensity to 57% is expected. Thus, the XPS observations are consistent with the abstraction of the TMS groups through breaking the bond of the Si to the alkynyl carbon. Furthermore, the XPS data confirm the desorption of the dominating part of the cleaved-off TMS groups as inferred from the STM data.

From the combined STM and XPS results it can be concluded that starting from 400 K, thermal annealing activates the abstraction of TMS moieties resulting in the formation of deprotected TEB molecules. The extended structures of reduced apparent height are attributed to polymerized TEB remains having formed an irregular, conjugated carbon structure. The embedded bright protrusions, whose relative abundance decreases with temperature, most likely represent a minority of remaining TMS groups.

2.1.2. Au(111)

Upon deposition onto a Au(111) surface kept at 200 K (Figure S5b), a higher diffusion rate afforded by the Au(111) surface in contrast to Cu(111) enables TMS-TEB molecules to self-assemble into dense-packed islands. Within these islands, a regular structural pattern consisting of molecules and hollow areas can be identified (Figure S5b inset), although the resolution does not afford a clear identification of the alignment of individual molecules. A minor part remains isolated and

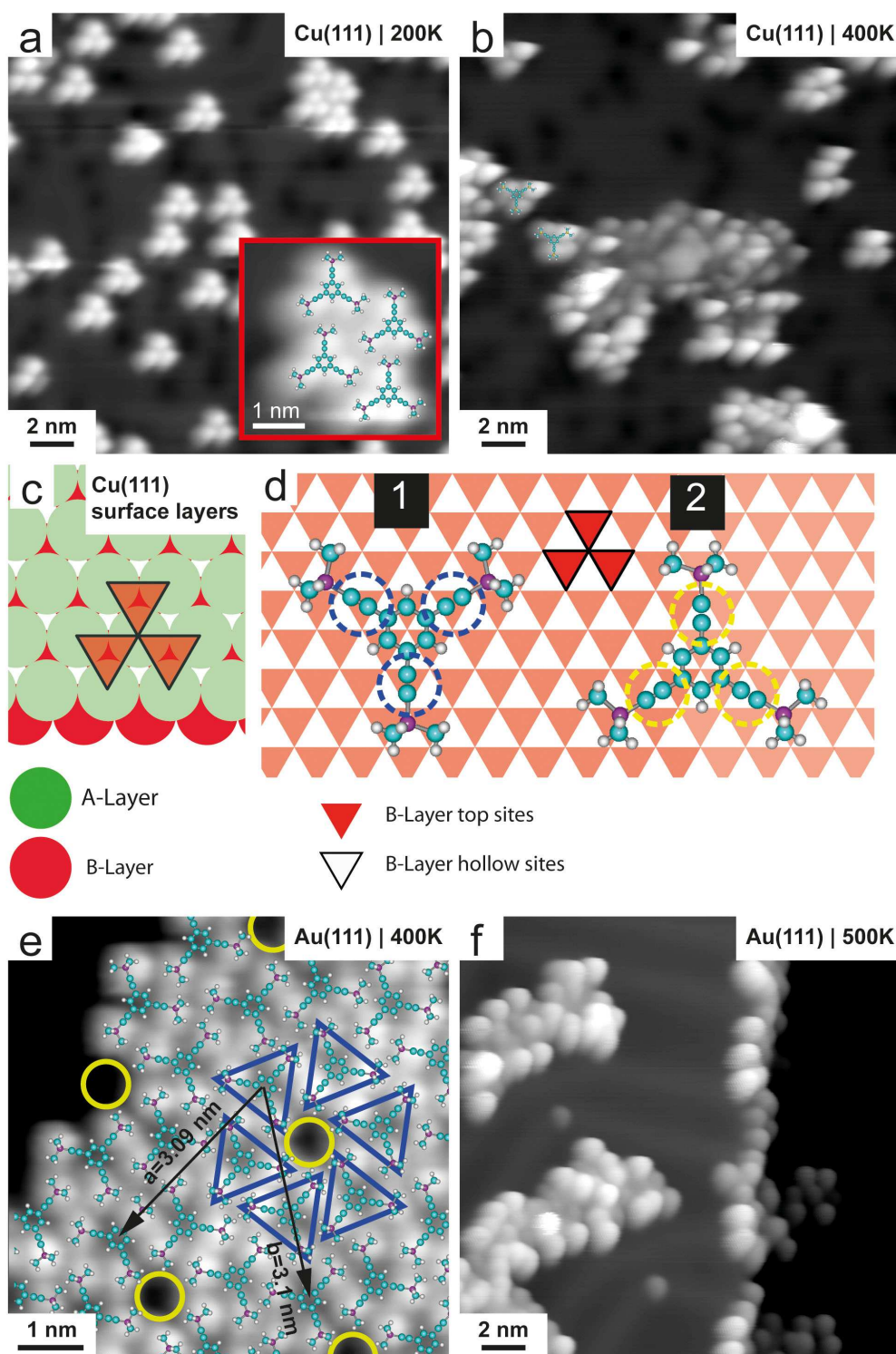


Figure 2. STM topographs of TMS-TEB: a) deposition onto Cu(111) held at 200 K ($I = 0.12 \text{ nA}$, $U = -1 \text{ V}$) and b) after annealing to 400 K ($I = 0.05 \text{ nA}$, $U = -1 \text{ V}$); c) model of the A- and B-layer of the Cu(111) surface; d) models with molecule overlays of TMS-TEB illustrating two distinct adsorption configurations; e) TMS-TEB on Au(111) after annealing to 400 K ($I = 0.1 \text{ nA}$, $U = -0.4 \text{ V}$) and f) after annealing to 500 K ($I = 0.09 \text{ nA}$, $U = -0.5 \text{ V}$).

preferentially adsorbs at the elbow-sites of the herringbone reconstruction lines of Au(111). After subsequent annealing to 400 K, the aggregated islands appear unchanged in the larger scale STM image, however, the reduction of isolated adsorbates

frequently interacting with the STM tip now allows to resolve their structure more clearly. Overlaid molecular models show that individual molecules are arranged in a hexagonal pattern consisting of six individual molecules with alternating orienta-

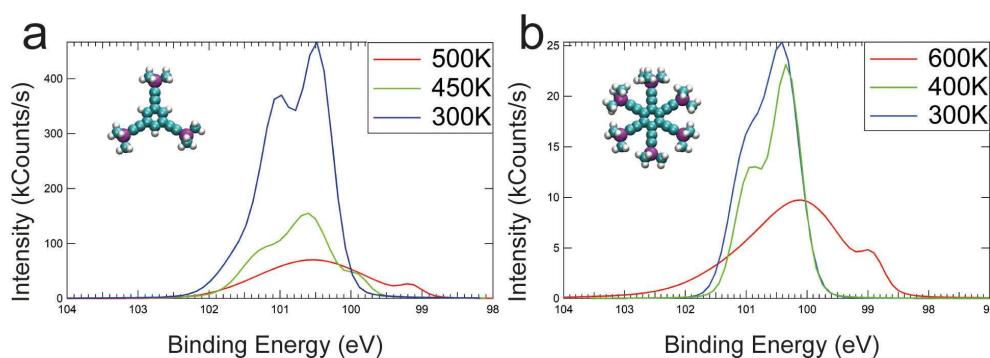


Figure 3. XPS: Si 2p spectra of a) TMS-TEB and b) TMS-HEB on Cu(111) after annealing to the indicated temperatures.

tions surrounding a small pore (Figure 2e). Thus, in contrast to the behavior on Cu(111), annealing to 400 K is not sufficient to trigger TMS abstraction.

Annealing to 500 K (Figure 2f) leads to obvious changes of the molecular adlayer. The adsorbates now appear in irregular islands comprising both darker and brighter features closely connected, which resembles much the case on Cu(111). Thus, again we attribute the observed transformation to the deprotection of the alkyne groups. Upon further annealing to 600 K (Figure S5c), the amount of bright features has decreased even more, indicating that at this temperature most TMS groups have been cleaved off and have desorbed from the surface. The remaining polymerized structures again are irregular.

2.2. TMS-Ext-TEB

As second molecule we investigated TMS-Ext-TEB (cf. Figure 1b), a heavier version of the previous species, i.e., we kept the three-fold symmetry, but added three more phenyl rings, thereby reaching a molecular weight of almost 600 g/mol.

2.2.1. Cu(111)

Upon deposition of the larger precursor onto Cu(111) kept at 200 K, scattered isolated units as well as small aggregates can be observed (Figure 4a). The organic units appear as triangle-shaped objects with a bright protrusion at each corner (Figure 4a inset). Again, the uniform appearance of the molecules demonstrates that TMS-Ext-TEB molecules adsorb on the surface as fully intact units. After annealing to 400 K (Figure 4b), the formation of densely-packed islands consisting of molecular species featuring a more uniform apparent height without terminal bright lobes can be observed aside a minority of smaller clusters with irregularly positioned molecules and containing impurities. A closer look at the islands (Figure 4b inset) reveals that the extent of the building blocks is consistent with assuming a molecular species where the TMS groups have been cleaved off. Furthermore, depressions in the apparent height of the metal surface can be identified near to the alkyne

groups. The packing scheme reproduces the previously reported geometry of triply dehydrogenated Ext-TEB,^[20,55] thus further supporting the abstraction of the TMS groups from the original precursor. We therefore conclude that these islands consist of precursors that have lost all TMS groups, but have interestingly not polymerized with each other due to strong bonding of the alkyne moieties to the substrate as suggested in previous work.^[20] This is in contrast to the smaller TMS-TEB, where deprotection of the smaller species resulted in less-ordered structures. This can be attributed to TMS-TEB being more reactive due to a higher relative content of reactive alkyne moieties in comparison to less reactive phenyl rings. Additionally, the phase space explored at the relevant temperature is larger for the smaller species as well. Consequently, more available reaction pathways for the smaller TMS-TEB lead to a larger variety of coupling motifs. For TMS-Ext-TEB, intermolecular coupling of supposedly covalent nature can be triggered by annealing to higher temperatures, whereby irregularly reticulated structures similar to those of TMS-TEB appear.

2.2.2. Au(111)

After evaporating TMS-Ext-TEB onto a Au(111) surface held at 200 K (Figure S7a), the majority of molecules forms densely-packed islands while individual units prefer adsorbing at the elbow-sites of the herringbone reconstruction lines. The individual molecules appear as triangle-shaped objects with bright features at each corner, again indicating their intactness. After annealing to 400 K (Figure 4c), TMS-Ext-TEB self-assembles into larger densely-packed islands, whereby the Au(111) chevron reconstruction is retained. Superpositioning molecular models allows the identification of individual units as their appearance remains unchanged, indicating that 400 K is insufficient to trigger TMS abstraction on Au(111). Annealing to 500 K (Figure 4d), however, yields visible changes as irregularly reticulated structures consisting of bright and darker features have formed. Since the embedded bright features are again attributed to the remaining TMS groups, it is still possible in a few cases to identify individual TMS-Ext-TEB units (green outline) despite the irregularity of the structure. Furthermore,

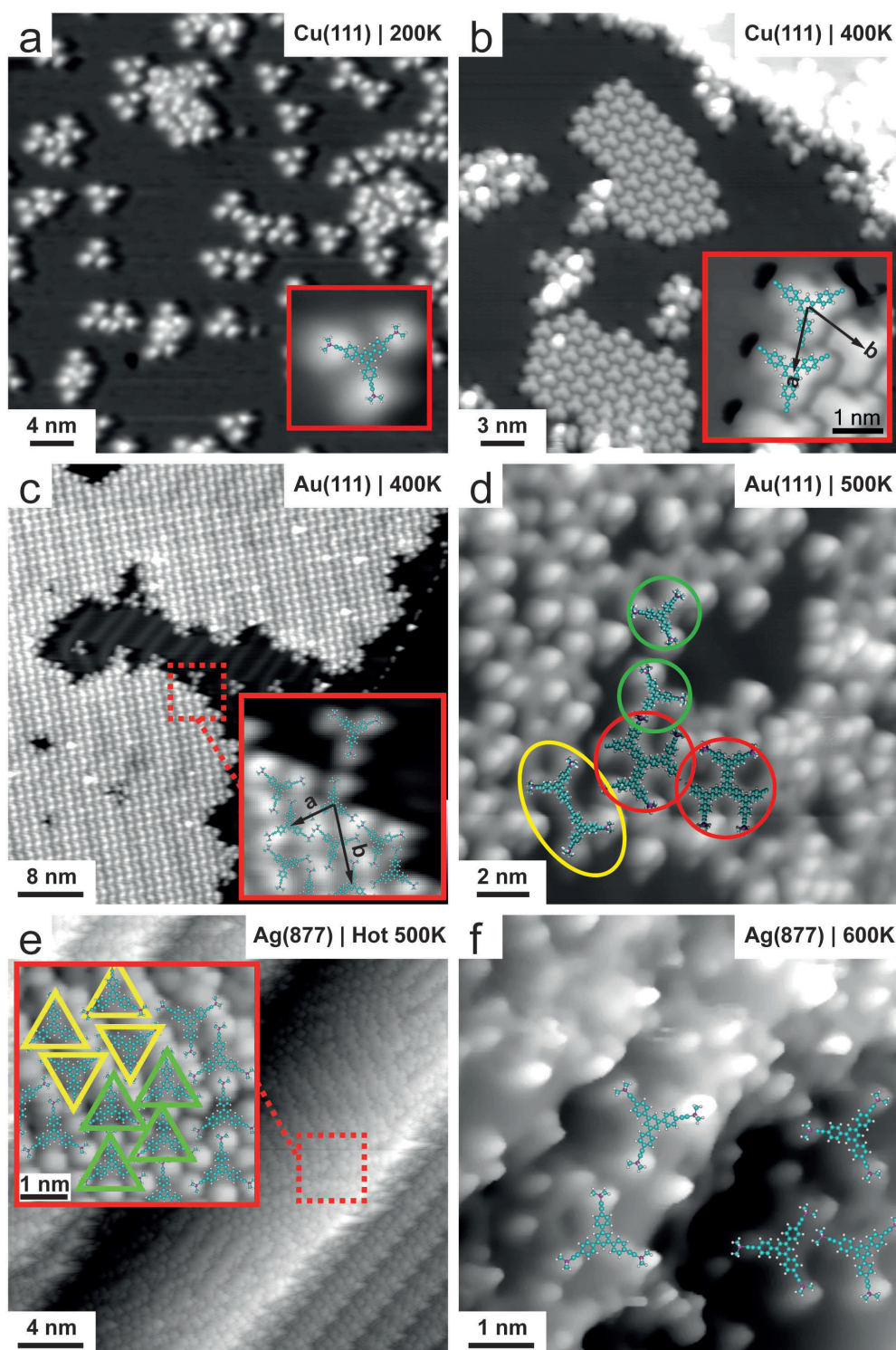


Figure 4. STM topographs of TMS-Ext-TEB: a) deposition on Cu(111) held at 200 K ($I=0.03$ nA, $U=-1$ V) and b) after annealing to 400 K ($I=0.5$ nA, $U=-1$ V); unit cell $a=1.35$ nm, $b=1.35$ nm c) TMS-Ext-TEB on Au(111) after annealing to 400 K ($I=0.09$ nA, $U=-0.4$ V); unit cell $a=1.29$ nm, $b=2.19$ nm, and d) after annealing to 500 K ($I=0.12$ nA, $U=-0.27$ V) e) TMS-Ext-TEB after hot deposition on Ag(877) held at 500 K ($I=0.02$ nA, $U=1$ V) and f) after subsequent annealing to 600 K ($I=0.16$ nA, $U=0.29$ V); green, yellow and red outlines in d) mark intact TMS-Ext-TEB, partially deprotected species, and oligomers with an appearance consistent with assuming cyclotrimerization, respectively.

other distinct object with reduced apparent height can be observed. Superpositioning molecular models indicates that some of these species are made up of singly deprotected

molecules (yellow outlines), suggesting the onset of TMS abstraction at 500 K. This is further supported by the occurrence of structures (red outlines) which we tentatively assign to

cyclotrimerized products as their shape and appearance are in line with previous results.^[27] Related three-fold coupling motifs have been recently reported for precursors carrying hydrogen-terminated alkynes on the same surface.^[26,41] Here, however, the exact chemical nature of the newly formed C₆ ring remains unclear. After further annealing to 650 K, the irregular structures express an almost uniform height, whereby only a small amount of bright features remains embedded (Figure S7b). We attribute the reticulated structures to the formation of a conjugated carbon network in which the few remaining features represent a small amount of remaining TMS groups.

2.2.3. Ag(877)

With respect to reactivity, Cu and Au are generally considered to be the most and the least reactive of the coinage metals, respectively. Since we were interested how Ag would behave in comparison, TMS-Ext-TEB was evaporated on the Ag(877) surface, a vicinal surface with (111) facets separated by regular atomic steps. After adsorption at room temperature it is observed that individual molecules adsorb preferentially at the step edges or form densely-packed islands (Figure S7c). Similar to the previously discussed Au(111) surface, mild annealing to 400 K does not lead to significant changes (Figure S7d) and is therefore insufficient for triggering TMS abstraction, though with the many step edges being preferred adsorption sites, a detailed analysis is difficult. Annealing to temperatures higher than 400 K results in desorption of the adsorbates and thus prevents a straight-forward determination of the TMS activation temperature on silver. However, following hot deposition of TMS-Ext-TEB with a very high flux onto a Ag(877) surface kept at 500 K, a monolayer coverage can be achieved (Figure 4e) despite the higher substrate temperature. Superpositioning molecular models indicates that, despite the preparation using high flux and high temperatures, individual intact units can still be identified as triangle-shaped objects with bright features at each corner. A closer look at the molecular arrangement reveals domains with different packing schemes: domains consisting of molecules with the same orientation (green) and domains consisting of molecules with alternating orientation (yellow) (Figure 4e inset). Subsequent annealing to 600 K (Figure 4f) leads to desorption as the number of molecules visibly decreases. Notably, superpositioned molecular models indicate that a significant portion of the remaining molecules is still fully intact. However, since the appearance of the molecules has changed as not every feature can be clearly assigned to an individual molecule anymore, while not providing unambiguous proof, it suggests that deprotection has started to occur. This shows however, that on Ag(877), TMS groups stay inert at temperatures above 500 K up to temperatures of almost 600 K, at which point notable molecule desorption has already begun. Therefore, our data reveals that with respect to TMS group deprotection, the Ag surface appears to be even more unreactive than the Au surface. The influences of the various surfaces on the reaction pathways of alkyne moieties have been discussed in the literature,^[14,56–58] however knowledge on TMS-

abstraction is missing. Based on our findings, we tentatively attribute the higher activity of Au to the larger amount of surface state electrons contributing to the surface-adsorbate interaction seemingly weakening the alkynyl-TMS bond.

2.3. TMS-HEB

The motivation for the third precursor was to study a similarly heavy species compared to the previous one carrying a larger number and more-closely positioned alkyne groups, which might affect the activation behavior. Therefore, we synthesized TMS-HEB (cf. Figure 1c), featuring one central phenyl ring surrounded by six alkynyl-TMS groups and a mass of 655 g/mol.

2.3.1. Cu(111)

Upon deposition onto a surface kept at 200 K (Figure 5a), TMS-HEB molecules self-assemble into densely packed islands with the same symmetry as the underlying substrate. The larger extent of the islands compared to TMS-TEB and TMS-Ext-TEB indicates an increased mobility for the species with six alkynyl-TMS groups. This is intriguing, since the strongest interaction with the substrate is typically mediated through the ethynyl groups.^[20,48,57] We tentatively rationalize the reduction of surface interaction with increasing the number of reactive groups with the spacing of the triple bonds being unfavorable for the Cu epitaxy as, in contrast to TMS-TEB, attempting to replicate the same adsorption geometry for TMS-HEB would not result in all ethynyl groups placed at favorable adsorption sites but in three ethynyl groups placed at favorable and three at unfavorable adsorption sites (Figure 5d). This scenario is expected to result in a reduction of the energy barriers between neighboring adsorption sites relevant for the diffusion processes. Following the same procedure as with the previous molecules, a superposition of molecular models (Figure 5a inset) shows that fully intact individual molecules appear as hexagonal-shaped objects with a bright feature at each corner. This is congruent with the six-fold symmetry of the molecule.

After annealing to 400 K (Figure 5b), the previously dense-packed islands transform into irregular structures, whereby it is hard to identify whether they contain intermolecular covalent linkages. In contrast, it is obvious that aside intact adsorbates (green) also species with four (orange) and three (red) bright lobes are present, suggesting that either two or three TMS groups, respectively, have been abstracted in some cases. This is supported by the XPS data of the Si 2p spectrum (Figure 3b), showing that the integrated counts start to decrease for a sample annealed to 400 K (green curve). After further annealing to 600 K, irregular structures with almost uniform height containing small amounts of bright features have formed (Figure S8a). Again, this can be attributed to the formation of a conjugated carbon backbone while the few remaining features represent a small amount of unabstracted TMS groups. The XPS confirms this interpretation by expressing a broader signature (red curve) carrying contributions from atomic and various

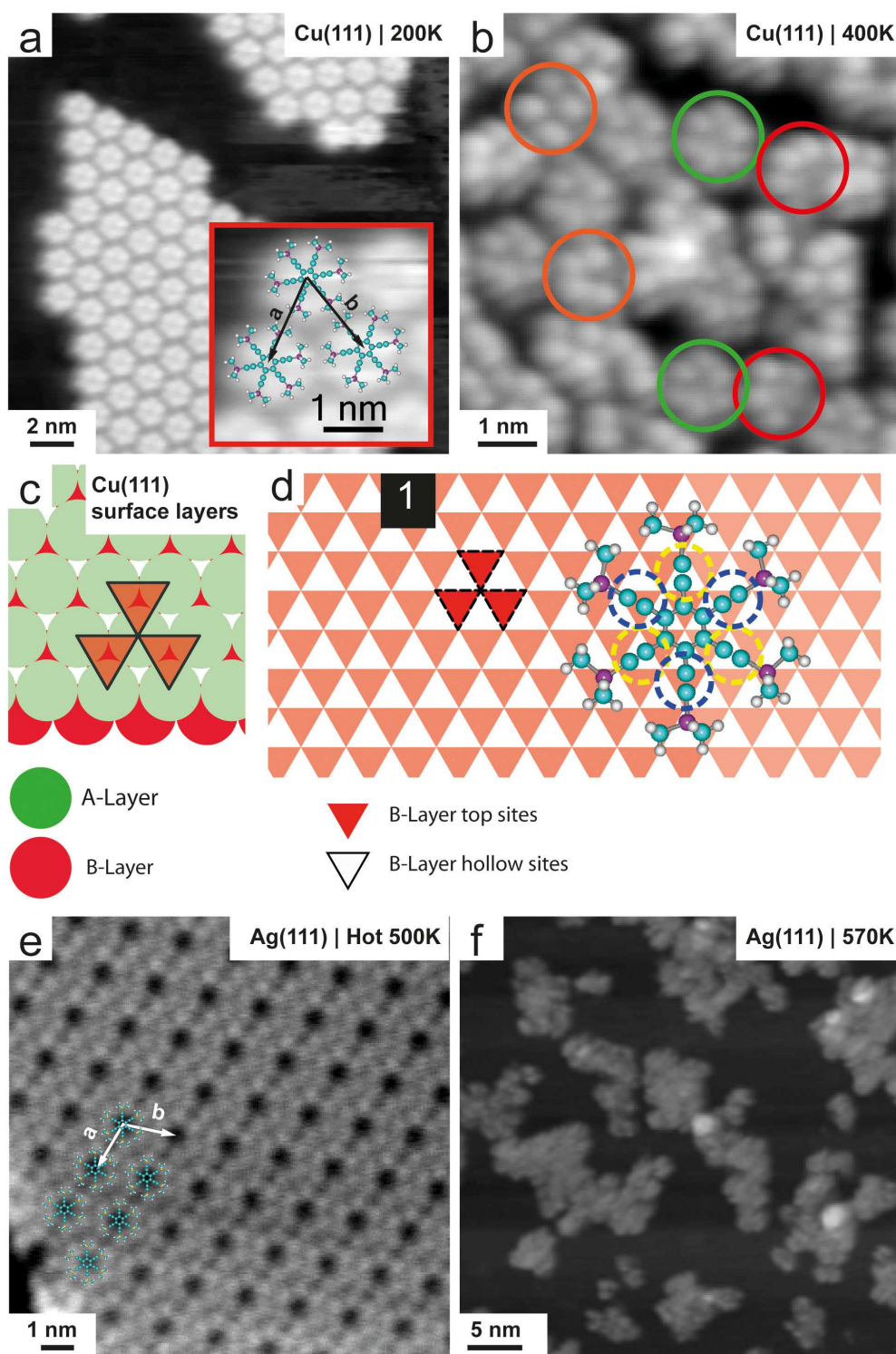


Figure 5. STM topographs of TMS-HEB: a) after deposition onto Cu(111) held at 200 K ($I = 0.08$ nA, $U = -0.65$ V); unit cell $a = 1.58$ nm, $b = 1.57$ nm; and b) after annealing to 400 K ($I = 0.077$ nA, $U = -0.85$ V); green circles: fully intact molecules; orange circles: molecules with four TMS groups; red circles: molecules with three TMS groups; c) model of the A- and B-layer of the Cu(111) surface; d) illustration of adsorption configuration for TMS-HEB; e) TMS-HEB after hot deposition onto Ag(111) held at 500 K ($I = 0.1$ nA, $U = -0.5$ V); unit cell $a = 1.65$ nm, $b = 1.65$ nm; and f) subsequent annealing to 570 K ($I = 0.05$ nA, $U = -0.5$ V).

molecular silicon species (Figure 3b). The reduction of the integrated Si 2p intensity is less prominent as in the case of TMS-TEB which is fully consistent with the large amount of

remaining bright features being distinguishable in the STM data of TMS-HEB (Figure S8a).

2.3.2. Ag(111)

At 200 K (Figure S8b), intact TMS-HEB molecules self-assemble in a closely-related fashion compared to that on Cu(111) and the intact molecules also express a similar appearance. Subsequent annealing to 400 K and 500 K leads to strong molecule desorption, as was the case with TMS-Ext-TEB on Ag(877). However, by depositing molecules with a high flux onto a Ag (111) surface kept at 500 K, an almost full monolayer of intact molecules self-assembled into densely-packed domains can be achieved (Figure 5e). Annealing this sample to 570 K (Figure 5f) results in desorption of a part of the adsorbates combined with a conversion of the remaining part whereby the previously densely-packed domains turn into irregular aggregates. Even though it remains unclear if the conversion includes abstraction of TMS groups or mainly transforms the alkyne moieties, our data demonstrate that TMS protected alkyne derivative stay intact to comparably high temperatures beyond 500 K.

2.4. TMS-Ext-HEB

The next species was designed to investigate the limits of compatibility with the OMBE process for heavy TMS derivatives. The TMS-Ext-HEB species (cf. Figure 1d) features seven phenyl rings and six alkynyl-TMS groups and has a weight of more than 1100 g/mol.

2.4.1. Cu(111)

Upon adsorption onto the substrate kept at 200 K, TMS-Ext-HEB units aggregate into loosely ordered clusters and smaller patches locally expressing complex patterns (Figure 6a). Individual intact molecules (species 1) can be identified at the outer edge of the islands as hexagonal-shaped objects with bright features at each corner by superpositioning molecular models (Figure 6a inset). While the image doesn't prove that all molecules must be intact, the regular parts indicate that the dominating portion of precursors are unchanged. After annealing to 450 K (Figure 6b), in addition to clusters consisting of circular objects with a few embedded bright features, scattered isolated circular objects can also be observed. The often isolated occurring species 2 has a clear internal structure, while species 3, typically related to the clusters, expresses a featureless, uniform oval. By superpositioning molecular models (Figure 6c), we attribute species 2 to a fully activated precursor that has yet to be cyclodehydrogenated. The latter species 3 is rationalized by being a fully deprotected and cyclodehydrogenated compound. Related processes have been reported before, e.g., for an oxygen-terminated Ext-HEB species.^[13,59] In either case, the analysis evidences that TMS groups have been fully abstracted.

2.4.2. Au(111)

After room temperature deposition, TMS-Ext-HEB adsorbates have self-assembled into densely packed extended and chiefly ordered islands (Figure 6d). The inset with the molecular overlays show that the observed pattern is consistent with a domain containing intact precursors. Although individual molecules cannot be assigned, translationally repeating units in the forms of a bowtie (yellow and green) with two different orientations can be identified. The unit cell exhibits the shape of a rhomboid with unit cell dimensions $a = 2.42$ nm and $b = 6.12$ nm. After annealing to 550 K, the prominent changes of the adlayer morphology evidence that TMS activation has occurred (Figure 6e). Intramolecular contrast originating from the six TMS groups is hardly discernible anymore. The fact that most molecules have taken on the form of uniform round shapes suggests that they underwent cyclodehydrogenation. At the same time, a reduction of the molecule coverage can be observed. Further annealing to 650 K affords almost full activation leading to polymerized structures, as the majority of bright features has disappeared (Figure S9).

3. Conclusions

We systematically explored organic precursors featuring TMS-protected alkyne moieties as functional groups regarding their potential as building blocks for on-surface synthesis. We were able to evaporate various species with molecular weights ranging from 366 g/mol to over 1100 g/mol onto surfaces without signs of molecular deterioration. Thus our results demonstrate that regarding the evaporation process the TMS functional group acts as protection group that reduce intermolecular reactions during the OMBE process even for heavier alkyne precursors. Therefore, TMS-functionalization of the alkynyl group overcomes an obstacle previously limiting the use of building blocks featuring terminal alkynes under UHV conditions.

Furthermore, our study revealed the onset temperatures for deprotection of the TMS-terminated alkyne derivatives on different coinage metal substrates (Table 2). Whether the func-

Table 2. Overview of the onset temperature for deprotection of the TMS-terminated alkyne derivatives on the different substrates. Temperatures in parentheses for silver substrates indicate that the particular species stayed inert up to that temperature. The acquired data hints at deprotection occurring above that temperature, but does not provide definite proof as considerable molecule desorption interferes.

Molecule	Substrates			
	Cu(111)	Au(111)	Ag(111)	Ag(877)
TMS-TEB	400 K	500 K	–	–
TMS-Ext-TEB	400 K	500 K	–	(\approx 550 K)
TMS-HEB	400 K	–	(\approx 550 K)	–
TMS-Ext-HEB	450 K	500 K	–	–

tional moieties act as leaving or protecting groups depends on the choice of the substrate. On copper or gold surfaces, TMS

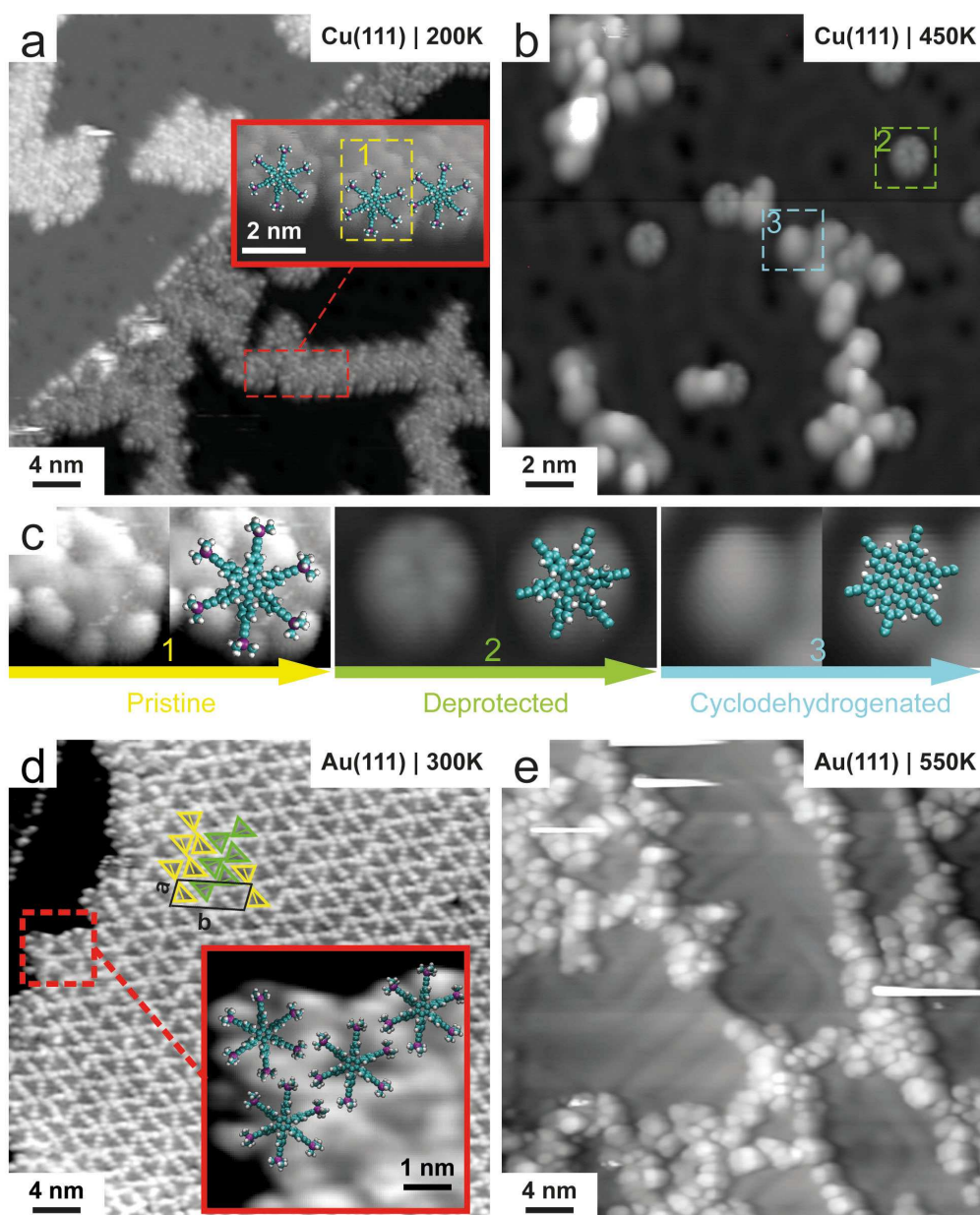


Figure 6. STM topographs of TMS-Ext-HEB: a) after deposition onto Cu(111) held at 200 K ($I=0.09$ nA, $U=-0.47$ V); inset: pristine molecule is marked with 1 (yellow) and b) after annealing to 450 K ($I=0.1$ nA, $U=-0.1$ V); deprotected molecules species and further cyclodehydrogenated species are marked by 2 (green) and 3 (cyan), respectively; c) molecule transformation progression; yellow: pristine molecule (1 left) with additionally overlaid model (1 right); green: deprotected molecule (2 right) with additionally overlaid model (2 right); cyan: further cyclodehydrogenated molecule (3 left) with additionally overlaid model (3 right); d) after deposition onto Au(111) held at 300 K ($I=0.11$ nA, $U=-0.87$ V); unit cell $a=2.42$ nm, $b=6.12$ nm; yellow and green bowtie shapes indicate two different translationally repeating units; and e) after subsequent annealing to 550 K ($I=0.065$ nA, $U=-0.77$ V).

groups can be abstracted by thermal annealing to 400 K and 500 K, respectively. Both STM and XPS data consistently demonstrate that the dominating part of the cleaved-off TMS moieties desorbs from the surface. This means that, in contrast to the commonly used halides, utilizing TMS groups as leaving groups on copper and gold surfaces is a nearly residue-free process. By contrast, on close-packed silver surfaces, the functional groups withstand thermal annealing up to almost 550 K, at which point forward significant molecule desorption begins, and thus can be considered efficient protecting groups.

The combination of these two characteristics makes the utilization of TMS groups a simple-to-use method that on the one hand not only increases the variety of alkyne precursors that can be evaporated via organic molecular beam epitaxy, but on the other, also may deliver more flexibility for reaction pathway control as the leaving or protecting character of TMS groups can be controlled by the appropriate choice of substrates and preparation protocols. Specifically the combination with other functional groups whose activation temperature differs from that of TMS protected alkynes is expected to render

control over hierarchic reaction pathways and thus expresses potential for future on-surface synthesis protocols.

Acknowledgement

The authors thank C. Wöll and A. Nefedov for providing access to the HE-SGM end station. The authors acknowledge funding by the German Research Foundation (DFG) Excellence Cluster Munich Center for Advanced Photonics, the International Max-Planck Research School of Advanced Photon Science (IMPRS-APS), the TUM Institute of Advanced Studies, DFG projects KL 2294/3-1, KL 2294/6-1, National Natural Science Foundation of China Grant (No. 21802067), and ERC Advanced Grant MolArt (no. 247299). M.R. acknowledges support by the DFG-priority programs 1459, TR88 "3Met" and the KNMF facility (KIT, Germany). The authors thank the Helmholtz-Zentrum Berlin-Electron storage ring BESSY II for provision of synchrotron radiation at the beamline HE-SGM.

Conflict of Interest

The authors declare no conflict of interest.

Keywords: alkyne · on-surface reaction · protecting groups · scanning tunneling microscopy · trimethylsilyl

- [1] A. Hirsch, *Nat. Mater.* **2010**, *9*, 868–871.
 [2] F. Diederich, M. Kivala, *Adv. Mater.* **2010**, *22*, 803–812.
 [3] J. Méndez, M. F. López, J. A. Martín-Gago, *Chem. Soc. Rev.* **2011**, *40*, 4578.
 [4] Y. Y. Li, L. Xu, H. Liu, Y. Y. Li, *Chem. Soc. Rev.* **2014**, *43*, 2572–2586.
 [5] N. Narita, S. Nagai, S. Suzuki, K. Nakao, *Phys. Rev. B* **1998**, *58*, 11009–11014.
 [6] H. Tang, C. M. Hessel, J. Wang, N. Yang, R. Yu, H. Zhao, D. Wang, *Chem. Soc. Rev.* **2014**, *43*, 4281–4299.
 [7] L. D. Pan, L. Z. Zhang, B. Q. Song, S. X. Du, H.-J. Gao, *Appl. Phys. Lett.* **2011**, *98*, 173102.
 [8] Z. Chen, C. Molina-Jirón, S. Klyatskaya, F. Klappenberger, M. Ruben, *Ann. Phys.* **2017**, *529*, 1700056.
 [9] L. Gross, F. Moresco, P. Ruffieux, A. Gourdon, C. Joachim, K.-H. Rieder, *Phys. Rev. B* **2005**, *71*, 165428.
 [10] L. Grill, M. Dyer, L. Lafferentz, M. Persson, M. V. Peters, S. Hecht, *Nat. Nanotechnol.* **2007**, *2*, 687–691.
 [11] J. V. Barth, *Annu. Rev. Phys. Chem.* **2007**, *58*, 375–407.
 [12] J. Cai, P. Ruffieux, R. Jaafar, M. Bieri, T. Braun, S. Blankenburg, M. Muoth, A. P. Seitsonen, M. Saleh, X. Feng, K. Müllen, R. Fasel, *Nature* **2010**, *466*, 470–473.
 [13] M. Treier, C. A. Pignedoli, T. Laino, R. Rieger, K. Müllen, D. Passerone, R. Fasel, *Nat. Chem.* **2011**, *3*, 61–67.
 [14] H.-Y. Gao, J.-H. Franke, H. Wagner, D. Zhong, P.-A. Held, A. Studer, H. Fuchs, *J. Phys. Chem. C* **2013**, *117*, 18595–18602.
 [15] M. Koch, M. Gille, A. Viertel, S. Hecht, L. Grill, *Surf. Sci.* **2014**, *627*, 70–74.
 [16] F. Klappenberger, Y.-Q. Zhang, J. Björk, S. Klyatskaya, M. Ruben, J. V. Barth, *Acc. Chem. Res.* **2015**, *48*, 2140–2150.
 [17] Y. He, M. Garnica, F. Bischoff, J. Ducke, M.-L. Bocquet, M. Batzill, W. Auwärter, J. V. Barth, *Nat. Chem.* **2017**, *9*, 33–38.
 [18] Q. Li, B. Yang, H. Lin, N. Aghdassi, K. Miao, J. Zhang, H. Zhang, Y. Li, S. Duhm, J. Fan, L. Chi, *J. Am. Chem. Soc.* **2016**, *138*, 2809–2814.
 [19] T. Lin, Y.-Q. Zhang, L. Zhang, F. Klappenberger, In *Encycl. Interfacial Chem.*, pages 324–334. Elsevier, **2018**.
 [20] Y.-Q. Zhang, J. Björk, P. Weber, R. Hellwig, K. Diller, A. C. Papageorgiou, S. C. Oh, S. Fischer, F. Allegretti, S. Klyatskaya, M. Ruben, J. V. Barth, F. Klappenberger, *J. Phys. Chem. C* **2015**, *119*, 9669–9679.
 [21] Y.-Q. Zhang, N. Kepčija, M. Kleinschrodt, K. Diller, S. Fischer, A. C. Papageorgiou, F. Allegretti, J. Björk, S. Klyatskaya, F. Klappenberger, M. Ruben, J. V. Barth, *Nat. Commun.* **2012**, *3*, 1286.
 [22] H.-Y. Gao, H. Wagner, D. Zhong, J.-H. Franke, A. Studer, H. Fuchs, *Angew. Chem. Int. Ed.* **2013**, *52*, 4024–4028; *Angew. Chem.* **2013**, *125*, 4116–4120.
 [23] V. K. Kanuru, G. Kyriakou, S. K. Beaumont, A. C. Papageorgiou, D. J. Watson, R. M. Lambert, *J. Am. Chem. Soc.* **2010**, *132*, 8081–8086.
 [24] C. Sanchez-Sanchez, N. Orozco, J. P. Holgado, S. K. Beaumont, G. Kyriakou, D. J. Watson, A. R. Gonzalez-Elipse, L. Feria, J. F. Sanz, R. M. Lambert, *J. Am. Chem. Soc.* **2015**, *137*, 940–947.
 [25] T. Wang, J. Huang, H. Lv, Q. Fan, L. Feng, Z. Tao, H. Ju, X. Wu, S. L. Tait, J. Zhu, *J. Am. Chem. Soc.* **2018**, *140*, 13421–13428.
 [26] J. Liu, P. Ruffieux, X. Feng, K. Müllen, R. Fasel, *Chem. Commun.* **2014**, *50*, 11200–11203.
 [27] R. Hellwig, M. Uphoff, T. Paintner, J. Björk, M. Ruben, F. Klappenberger, J. V. Barth, *Chem. Eur. J.* **2018**, *24*, 16126–16135.
 [28] H.-Y. Gao, P. A. Held, S. Amirjalayer, L. Liu, A. Timmer, B. Schirmer, O. Diaz Arado, H. Mönig, C. Mück-Lichtenfeld, J. Neugebauer, A. Studer, H. Fuchs, *J. Am. Chem. Soc.* **2017**, *139*, 7012–7019.
 [29] T. Wang, H. Lu, Q. Fan, L. Feng, X. Wu, J. Zhu, *Angew. Chem. Int. Ed.* **2017**, *56*, 4762–4766; *Angew. Chem.* **2017**, *129*, 4840–4844.
 [30] P. B. Weber, R. Hellwig, T. Paintner, M. Lattelais, M. Paszkiewicz, P. C. Aguilar, P. S. Deimel, Y. Guo, Y.-Q. Zhang, F. Allegretti, A. C. Papageorgiou, J. Reichert, S. Klyatskaya, M. Ruben, J. V. Barth, M.-L. Bocquet, F. Klappenberger, *Angew. Chem. Int. Ed.* **2016**, *55*, 5754–5759; *Angew. Chem.* **2016**, *128*, 5848–5853.
 [31] J. Liu, X. Fu, Q. Chen, Y. Zhang, Y. Wang, D. Zhao, W. Chen, G. Q. Xu, P. Liao, K. Wu, *Chem. Commun.* **2016**, *52*, 12944–12947.
 [32] J. Liu, Q. Chen, L. Xiao, J. Shang, X. Zhou, Y. Zhang, Y. Wang, X. Shao, J. Li, W. Chen, G. Q. Xu, H. Tang, D. Zhao, K. Wu, *ACS Nano* **2015**, *9*, 6305–6314.
 [33] P. A. Held, H.-Y. Gao, L. Liu, C. Mück-Lichtenfeld, A. Timmer, H. Mönig, D. Barton, J. Neugebauer, H. Fuchs, A. Studer, *Angew. Chem. Int. Ed.* **2016**, *55*, 9777–9782; *Angew. Chem.* **2016**, *128*, 9929–9934.
 [34] T. Wang, Q. Fan, L. Feng, Z. Tao, J. Huang, H. Ju, Q. Xu, S. Hu, J. Zhu, *ChemPhysChem* **2017**, *18*, 3329–3333.
 [35] J. Liu, Q. Chen, Q. He, Y. Zhang, X. Fu, Y. Wang, D. Zhao, W. Chen, G. Q. Xu, K. Wu, *Phys. Chem. Chem. Phys.* **2018**, *20*, 11081–11088.
 [36] Y.-Q. Zhang, M. Paszkiewicz, P. Du, L. Zhang, T. Lin, Z. Chen, S. Klyatskaya, M. Ruben, A. P. Seitsonen, J. V. Barth, F. Klappenberger, *Nat. Chem.* **2018**, *10*, 296–304.
 [37] B. Cirera, Y.-Q. Zhang, J. Björk, S. Klyatskaya, Z. Chen, M. Ruben, J. V. Barth, F. Klappenberger, *Nano Lett.* **2014**, *14*, 1891–1897.
 [38] Q. Sun, L. Cai, H. Ma, C. Yuan, W. Xu, *ACS Nano* **2016**, *10*, 7023–7030.
 [39] F. Klappenberger, R. Hellwig, P. Du, T. Paintner, M. Uphoff, L. Zhang, T. Lin, B. A. Moganaki, M. Paszkiewicz, I. Vobornik, J. Fujii, O. Fuhr, Y.-Q. Zhang, F. Allegretti, M. Ruben, J. V. Barth, *Small* **2018**, *14*, 1704321.
 [40] B. Cirera, Y.-Q. Zhang, S. Klyatskaya, M. Ruben, F. Klappenberger, J. V. Barth, *ChemCatChem* **2013**, *5*, 3281–3288.
 [41] H. Zhou, J. Liu, S. Du, L. Zhang, G. Li, Y. Zhang, B. Z. Tang, H.-J. Gao, *J. Am. Chem. Soc.* **2014**, *136*, 5567–5570.
 [42] P. G. M. Wuts, T. W. Greene, *Greene's Protective Groups in Organic Synthesis*. John Wiley & Sons, Inc., Hoboken, NJ, USA, **2006**.
 [43] M. Yoshikawa, Y. Tamura, R. Wakabayashi, M. Tamai, A. Shimajima, K. Kuroda, *Angew. Chem. Int. Ed.* **2017**, *56*, 13990–13994; *Angew. Chem.* **2017**, *129*, 14178–14182.
 [44] T. X. Neenan, G. M. Whitesides, *J. Org. Chem.* **1988**, *53*, 2489–2496.
 [45] J. Eichhorn, W. M. Heckl, M. Lackinger, *Chem. Commun.* **2013**, *49*, 2900.
 [46] J. A. Lipton-Duffin, O. Ivasenko, D. F. Perepichka, F. Rosei, *Small* **2009**, *5*, 592–597.
 [47] D. Prenzel, T. Sander, J. Gebhardt, H. Soni, F. Hampel, A. Görling, S. Maier, R. R. Tykwinski, *Chem. Eur. J.* **2017**, *23*, 1846–1852.
 [48] R. Hellwig, T. Paintner, Z. Chen, M. Ruben, A. P. Seitsonen, F. Klappenberger, H. Brune, J. V. Barth, *ACS Nano* **2017**, *11*, 1347–1359.
 [49] F. Cicoira, C. Santato, M. Melucci, L. Favaretto, M. Gazzano, M. Muccini, G. Barbarella, *Adv. Mater.* **2006**, *18*, 169–174.
 [50] B. H. Lee, S. H. Park, H. Back, K. Lee, *Adv. Funct. Mater.* **2011**, *21*, 487–493.
 [51] R. Ohmann, G. Levita, L. Vitali, A. De Vita, K. Kern, *ACS Nano* **2011**, *5*, 1360–1365.
 [52] A. S. Münch, M. Wölk, M. Malanin, K.-J. Eichhorn, F. Simon, P. Uhlmann, *J. Mater. Chem. B* **2018**, *6*, 830–843.
 [53] K. Diller, Y. Ma, Y. Luo, F. Allegretti, J. Liu, B. Z. Tang, N. Lin, J. V. Barth, F. Klappenberger, *Phys. Chem. Chem. Phys.* **2015**, *17*, 31117–31124.

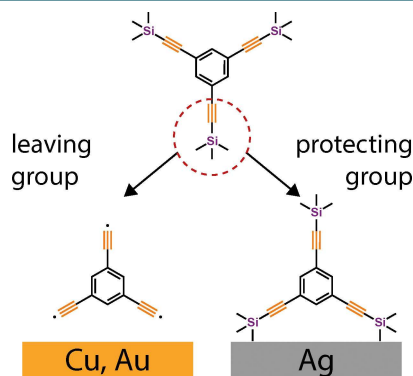
- [54] L. Dong, W. Wang, T. Lin, K. Diller, J. V. Barth, J. Liu, B. Z. Tang, F. Klappenberger, N. Lin, *J. Phys. Chem. C* **2015**, *119*, 3857–3863.
- [55] Y.-Q. Zhang, T. Paintner, R. Hellwig, F. Haag, F. Allegretti, P. Feulner, S. Klyatskaya, M. Ruben, A. P. Seitsonen, J. V. Barth, F. Klappenberger, *J. Am. Chem. Soc.* **2019**, *141*, 5087–5091.
- [56] J. Björk, Y.-Q. Zhang, F. Klappenberger, J. V. Barth, S. Stafström, *J. Phys. Chem. C* **2014**, *118*, 3181–3187.
- [57] T. Lin, L. Zhang, J. Björk, Z. Chen, M. Ruben, J. V. Barth, F. Klappenberger, *Chem. Eur. J.* **2017**, *23*, 15588–15593.
- [58] T. Wang, H. Lv, L. Feng, Z. Tao, J. Huang, Q. Fan, X. Wu, J. Zhu, *J. Phys. Chem. C* **2018**, *122*, 14537–14545.
- [59] K.s Weiss, G. Beernink, F. Dötz, A. Birkner, K. Müllen, C. H. Wöl, *Angew. Chem. Int. Ed.* **1999**, *38*, 3748–3752; *Angew. Chem.* **1999**, *111*, 3974–3978.

Manuscript received: March 13, 2019
 Revised manuscript received: May 14, 2019
 Accepted manuscript online: May 23, 2019
 Version of record online: ■■■, ■■■■

ARTICLES

Substrate dependent leaving or protecting group character of terminal trimethylsilyl moieties:

STM investigations of trimethylsilyl-protected alkyne precursors on coinage metal substrates unravel that the protecting or leaving group character of the terminal functional moieties can be controlled by an appropriate choice of substrates (Cu and Au vs. Ag) and preparation protocols. This affords new possibilities for control over hierarchic reaction pathways and thus expresses potential for future on-surface synthesis protocols.



L. Zhang, Dr. Y.-Q. Zhang, Dr. Z. Chen, Dr. T. Lin, M. Paszkiewicz, Dr. R. Hellwig, T. Huang, Prof. Dr. M. Ruben, Prof. Dr. J. V. Barth, Dr. F. Klappenberger*

1 – 13

On-Surface Activation of Trimethylsilyl-Terminated Alkynes on Coinage Metal Surfaces



Special Issue